Electronic structure of epitaxial Yb silicide

R. Hofmann, W. A. Henle, and F. P. Netzer*
Institut für Physikalische Chemie, Universität Innsbruck, A-6020 Innsbruck, Austria

M. Neuber
Fachbereich Physik, Universität Osnabrück, D-4500 Osnabrück, Germany
(Received 27 January 1992)

The formation of epitaxially ordered Yb silicide has been investigated by use of low-energy electron diffraction (LEED), Auger electron spectroscopy (AES), electron-energy-loss spectroscopy (EELS), and soft-x-ray photoemission spectroscopy (SXPS), and the epitaxial phases formed have been characterized by **k**-resolved uv photoemission spectroscopy (UPS) and inverse-photoemission spectroscopy (IPES). Thus, filled and empty electronic states as well as excitations between them have been assessed for various Yb silicide phases. The epitaxial Yb silicides have been prepared in two ways: by solid-state epitaxy of room-temperature-deposited Yb films on Si(111) via annealing, and by evaporation of Yb onto heated Si(111) substrates. The latter preparation method gave better ordering at lower temperatures. The phase diagram of the Yb-Si(111) interface has been established by AES and LEED, and from the $4f$ emission characteristics of the various surfaces in SXPS, a $YbSi_{2-x}$ phase is associated with the epitaxial (2×2) silicide. A structure model for this Yb silicide is suggested with a pure Si surface with ordered vacancies as the terminating layer. **k**-resolved UPS and IPES spectra are presented that demonstrate the order in the epitaxial silicide phase via complex dispersing features. A consistent interpretation of EELS results is based on the combined density-of-states results of UPS and IPES. Moreover, the EELS measurements add information on the morphology of the silicide phase via the plasmon behavior, which suggests an island-growth mechanism of the epitaxial silicide.

I. INTRODUCTION

The rare-earth (RE) silicides are intriguing materials with outstanding physicochemical and structural properties.[1,2] A number of rare-earth silicides grow in a defected AlB_2 structure with $RSi_{1.7}$ stoichiometry, which matches almost perfectly the lattice of the (111) surface of Si.[3] Consequently, epitaxially well-ordered phases of RE silicides have been observed to form from thin films of RE metals on Si(111) via solid-state epitaxy upon annealing the thin-film structures to elevated temperatures.[3–11] In one instance, ordered structures have also been detected by low-energy electron diffraction (LEED) for a RE silicide formed on a Si(100) substrate [Gd on Si(100)2×1], but the nature of this silicide and the morphology of the phase was less clear.[12]

Most of the RE silicides are good electrical and thermal conductors and metal-like with a relatively high density of states (DOS) at the Fermi level,[4,11] but there are exceptions to this pattern, e.g., Eu silicide[13] and, as we will report below, Yb silicide, which show a more semimetallic behavior with a low DOS at E_F. The majority of the RE silicides contain trivalent RE atoms with formally $(5d6s)^3$ valence-electron configurations but, again, an exception is Eu which remains divalent $[(5d6s)^2]$ throughout the Eu-Si interface phase diagram.[9] The most interesting case studied so far concerns the Yb silicides, which appear to adopt a valency according to stoichiometry: the Yb-rich silicide phases are mainly divalent, but the Si-rich phases become homogeneously mixed valent.[14] Braicovich *et al.*[15] have studied the formation of Yb silicides on low-coverage, thermally treated Yb-Si(111) interfaces using synchrotron radiation photoemission techniques, and have concentrated on the stoichiometries of the surface phases as a function of temperature by comparing Si $2p$ and Yb $4f$ photoemission results with those of bulk silicides; no mention was made of the observation of ordered silicide phases. Very recently, however, Wigren *et al.*[10] have reported the epitaxial growth of $YbSi_{2-x}$ on Si(111) 7×7 by solid-state epitaxy with annealing to 400 °C, and they determined a mean valency of 2.37 for the silicide from fittings of good quality $4f$ photoemission spectra.

The purpose of the present work was to perform a thorough study of the electronic structure of epitaxially grown Yb silicide by using uv photoelectron spectroscopy with synchrotron radiation in **k**-resolved form (angle-resolved uv photoemission), **k**-resolved uv inverse photoemission (IPES), and electron-energy-loss spectroscopy (EELS). Thus, the entire electronic structure, including filled and empty states, as well as electronic excitations between the two, have been assessed. Two methods of silicide preparation have been employed: solid-state epitaxy by annealing 10–50-monolayers- (ML) thick Yb films on Si(111) 7×7 to $\simeq500$ °C and, alternatively, Yb evaporation onto heated ($\simeq350$ °C) Si(111) substrates. The silicide phases have been characterized by soft-x-ray photoemission (SXPS), Auger electron spectroscopy (AES), and LEED, and a phase diagram of the Yb-Si(111) interface will be presented. We find that both methods of preparation yield the same stoichiometry and surface structure for the ordered silicide as judged from the AES Si- to

Yb-intensity ratios and LEED, but it appears that the silicide formed by evaporation onto the heated substrate exhibits better order. The temperature of formation of the ordered phase is lower in the latter case. Our SXPS results confirm the homogeneously mixed valent character of Yb disilicide as reported by Braicovich *et al.*[15] and Wigren *et al.*,[10] but we also observed purely divalent Yb-Si surface phases. Our $4f$ emission spectra allow us to propose a structure model for the disilicide, and the EELS spectra suggest an island-growth mechanism of the silicide phase.

II. EXPERIMENT

The experiments were carried out in two different UHV systems with base pressures $<10^{-10}$ mbar. One system contained a concentric hemispherical electron analyzer (Leybold EA 10) for AES and EELS measurements, a four-grid LEED optics (Omicron), and an IPES spectrometer. The latter consisted of an electrostatically focused electron gun with low angular divergence and a Geiger-Müller-type photon counter as described previously.[13] The detector accepts photons of 9.5 eV mean energy, and the overall energy resolution of the IPES system was measured to be $\simeq 0.35$ eV. The position of the electron gun with respect to the photon detector was fixed, but the sample surface could be rotated to obtain angular variations for **k**-resolved measurements. The second system was an angle-resolving electron spectrometer (VG ADES 400), which was attached to the TGM2 beamline of the synchrotron radiation laboratory Berliner Elektronenspeicherring-Gesellschaft für Synchrotronstrahlung m.b.h. (BESSY) in Berlin, Federal Republic of Germany.[16] The combined energy resolution for the photoemission measurements (monochromator plus analyzer) was typically ≤ 0.2 eV at low photon energies and $\simeq 0.3$ eV at $h\nu = 140$ eV.

Yb was evaporated onto clean, well-ordered Si(111)7×7 surfaces from W coils at ambient pressures $<8\times10^{-10}$ mbar. The clean Si surfaces (Si wavers, p-type, 1–2.5 Ω cm) were prepared by flashing the samples to 950 °C–1000 °C in a vacuum better than 3×10^{-10} mbar, and surface cleanliness and order was controlled by the existence of a sharp (7×7) LEED pattern, by AES, and by the existence of the Si(111)7×7-specific surface-state emissions in ultraviolet photoemission spectroscopy (UPS) and IPES. The Yb coverages were measured with quartz film thickness monitors (Inficon XTM), which were arranged in a similar geometry in the two experimental chambers. The Si wavers were heated by dc current and sample temperatures were established by reproducible current settings, which were calibrated against thermocouple readings and optical pyrometer observations in separate experiments. In the solid-state epitaxy experiments the substrates were held at the appropriate elevated temperatures for 5 min—this proved sufficient to saturate all the spectroscopic effects. After Yb evaporation the (7×7) surface could not be regained by flashing to high temperature and consequently a fresh sample was used for every experimental series.

III. RESULTS AND DISCUSSION

A. The phase diagram of the Yb-Si(111) interface

Figure 1 shows a three-dimensional representation of the phase diagram of the Yb-Si(111) interface as determined by AES and LEED. The Yb $N_{4,5}N_{6,7}N_{6,7}$ Auger peak amplitude at 180 eV has been plotted as a function of substrate temperature and Yb coverage; note that 1 ML Yb (1 RE atom per Si surface unit cell) corresponds to 3.2 Å. The AES signals have been normalized to equal sample current, and regions of ordered LEED structures are indicated in the figure, where each open circle represents an experimetal point. At low Yb coverages the Yb AES signal remains constant up to $\simeq 500$ °C, but for higher initial Yb coverages the Yb concentration of the surface region decreases steadily with increasing temperature, with a change of gradient between 500 °C and 600 °C. This is similar to what has been seen on the Eu-Si(111) interface,[9] but is in contrast to the Gd-Si(111) interface, where a plateau region of well-defined stoichiometry has been obtained.[16] Here, no stable plateau region in terms of stoichiometry and temperature can be observed. The coverage dependence of the Yb AES signal at room temperature saturates essentially at about 15–20 Å Yb, but the Si AES peak is still visible at very high Yb film thicknesses: after evaporation of 100 ML of Yb the Si AES can still be detected at room temperature, thus signaling a high rate of diffusion and solubility of Si in the Yb layer. After annealing, at $\simeq 350$ °C a (1×1) LEED structure becomes visible—note that ordered Si LEED structures disappear after evaporation of 1–2 Å Yb at room temperature—and for T in the range 500 °C–600 °C, a (2×2) LEED pattern is observed. This structure exists in a wide concentration range. Above 600 °C, the Yb content of the interface drops rapidly, and (5×1) and (3×1) LEED patterns can then been seen until a (1×1) structure prevails, except at low initial Yb coverages. In view of the very low Yb content of the interfacial region for $T > 700$ °C, the latter structures are considered as surface superstructures[17] rather than silicide phases.

The data points to the right of the main phase diagram in Fig. 1 show the Yb Auger amplitudes and the corresponding LEED structures after deposition of 50 Å Yb onto Si(111) kept at the elevated temperatures as indicated. Reproductions of LEED photographs are also given to illustrate the quality of order in these phases. As is evident from Fig. 1, the AES intensities are equal for the two experimental procedures, namely room-temperature evaporation plus annealing or evaporation onto substrates heated to the same temperature, and the chemical identity of the phases thus formed is therefore established. The LEED structures are also essentially the same. The LEED structures, however, appear at lower temperature [350 °C vs 500 °C for the (2×2)] for evaporation onto the heated sample. At 250 °C the (1×1) structure formed has additional weak $(\sqrt{3}\times\sqrt{3})R30°$ spots. We emphasize, though, that better ordering at lower temperatures is obtained for the direct reaction of Yb with Si at elevated temperatures, which is induced by evaporation of Yb onto the heated Si surfaces.

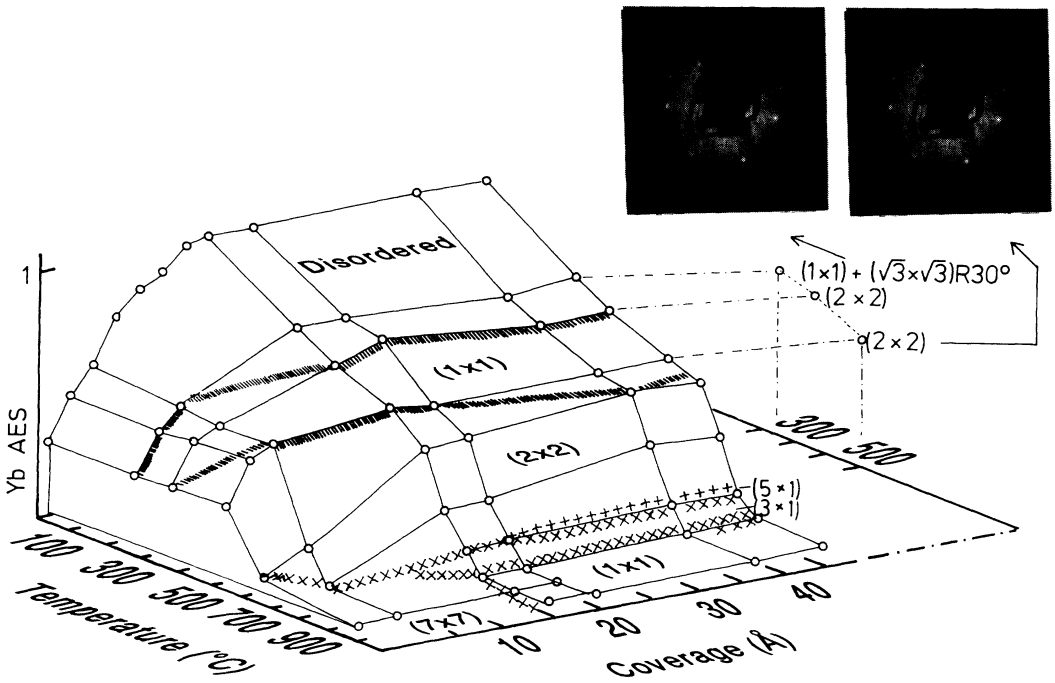

FIG. 1. Phase diagram of the Yb-Si(111) interface in the form of a plot of the Yb Auger signal vs temperature as a function of Yb coverage (1 monolayer is equal to 3.2 Å). Experimental points are symbolized by the open circles, and regions of ordered LEED structures are indicated. The data points to the right of the main three-dimensional diagram have been obtained by evaporation of 50 Å Yb onto heated Si substrates. The LEED photographs have been taken from these latter phases.

Si $2p$ and Yb $4f$ SXPS spectra of $\simeq 8$ ML Yb on Si(111) are shown in Fig. 2 to shed further light on the evolution of the Yb-Si interface with temperature and on the silicide formation process. The spectra have been recorded with a photon energy of 142 eV, and have been normalized to equal photon flux. The series of spectra on the right-hand side of Fig. 2 displays the valence region, which is dominated by the Yb $4f$ emissions as a result of cross-section effects at this photon energy.[18] For comparison, a spectrum of a metallic Yb surface, obtained from a thick Yb film on a Ta substrate, has been included in Fig. 2 (bottom curve). The $4f$ photoemission of metallic Yb shows the well-known spin-orbit doublet of the divalent Yb^{2+} $4f^{13}$ final-state configuration,[19] with a second doublet component, shifted to higher binding energy by 0.6 eV, attributed to the emission from the surface atoms.[20]

The $4f$ spectral profile of the 8-ML Yb-Si interface is significantly different from the metal spectrum, showing broader structure and a component closer to the Fermi edge. This indicates more than two components and, therefore, a degree of inhomogeneity in the interface. The corresponding Si $2p$ spectra are displayed on the left-hand side of Fig. 2. For the room-temperature interface, the Si $2p$ photoemission is shifted by 1.8 eV to lower binding energy with respect to the clean Si(111) surface (not shown), and such a chemical shift to lower binding energy is typical for Si in "reacted" RE-metal–Si interfaces.[9,12,15,16] The 8-ML Yb-Si room-temperature interface, however, still shows a spin-orbit-split Si $2p$ profile, thus indicating a defined interfacial reaction product, presumably in the form of an Yb-rich silicide. We note that the Yb is predominantly divalent in this room-temperature interfacial phase. Heating of the interface to $\simeq 250\,^{\circ}C$ produces pronounced spectral changes: the divalent $4f$ emission shifts towards E_F, multiplets of emission from trivalent Yb appear at 6–11 eV binding energy, and the Si $2p$ emission increases in intensity and shifts back to higher binding energy. This behavior is consistent with the formation of a phase that contains Yb in a valence-fluctuating configuration: both Yb^{2+} and Yb^{3+} multiplet states are present in the spectra, and the Yb^{2+} $4f$ states are *at the Fermi level,* allowing "energy-free fluctuations" of $4f$ and $5d6s$ valence states.[21]

Further heating introduces structural order into the interface, first a (1×1) structure at 350 °C and then a (2×2) structure between 500 °C and 600 °C is observed by LEED. The Si $2p$ emission shifts further to higher binding energy, and in the (2×2) structure it is at $\simeq 0.3$ eV to lower binding energy of the clean Si(111) 7×7 surface. The structural order is reflected in a sharper Si $2p$ profile, where the spin-orbit splitting is again clearly recognized. The profile sharpening is also apparent in the $4f$ emission, where a *single sharp doublet* at E_F with only a weak shoulder at $\simeq 3$ eV binding energy develops [see the spectrum of the (2×2) phase at 500 °C]. The $4f$ spectrum of the (2×2) structure agrees well with the corresponding spectrum of Wigren *et al.*[10] and, in accord with Abbati *et al.*,[14] is ascribed to an Yb disilicide ($YbSi_{2-x}$) phase. In the (1×1) phase the general appearance of the $4f$ profiles suggest a similar silicide, but the structural order is clearly less well developed at that stage.

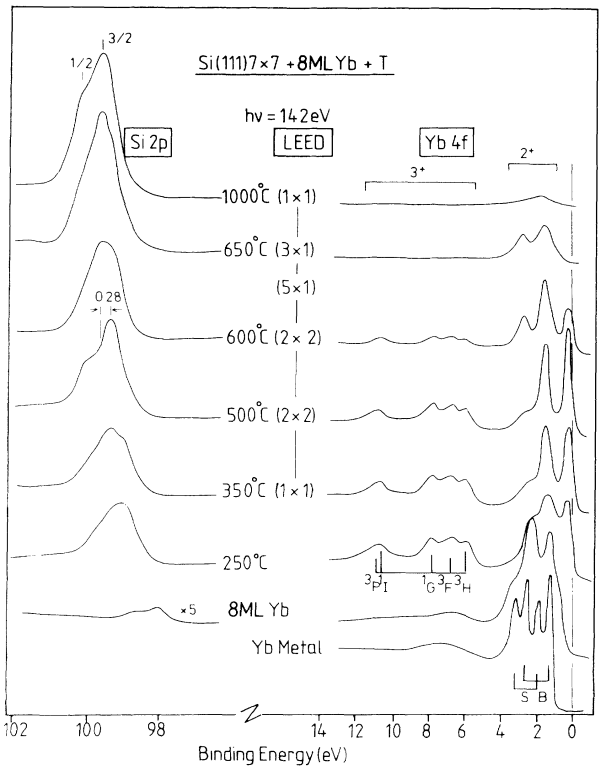

FIG. 2. X-ray-photoemission spectra of Si $2p$ core levels and of the Yb $4f$ region for 8 ML of Yb on Si(111) and for various phases formed by annealing of the room-temperature interface. The bottom curve of the right sequence is from metallic Yb, which has been recorded with $h\nu=60$ eV.

The preponderance of a single sharp $4f$ doublet structure and the absence of clear surface components in the photoemission spectrum of epitaxial Yb disilicide [see the spectrum of the 500 °C (2×2)] is unusual and interesting, and must be a reflection of the atomic surface environment. In analogy to epitaxially grown yttrium disilicide,[8] we propose that the surface of $YbSi_{2-x}$ is Si terminated with vacancies that are ordered into a (2×2) array. The fact that under certain conditions a $(\sqrt{3}\times\sqrt{3})$ structure is observed here as on YSi_{2-x} is consistent with that model, which incorporates all the Yb atoms in equivalent positions below the surface layer. Parenthetically, we note that the shoulder at $\simeq 3$ eV has been associated by Wigren *et al.*[10] with a divalent surface contribution; however, its intensity in Fig. 2 is too small as compared to that of the "mixed-valent bulk" component at E_F for this interpretation to hold. In view of the $4f$ evolution at higher temperatures, where a $4f$ component develops at the position of the 3-eV shoulder after decomposition of the disilicide, we conjecture that inhomogeneities in the disilicide layer may give rise to this extra $4f$ emission.

For annealing temperatures beyond 600 °C the Yb content of the interfacial region is markedly reduced, as already discussed above, and the dilution of Yb destroys the mixed-valent phases; the Yb $4f$ emission signals divalent Yb atoms at the surface in the resulting ordered (5×1) and (3×1) structures, and this confirms their superstructure character.

B. k-resolved uv photoemission and inverse photoemission

In order to probe the valence states of the Yb-Si system without interference from $4f$ states and to match the UPS spectra to the isochromat energy of IPES, low photon energies have to be employed. At photon energies around 10 eV the matrix elements for $4f$ photoionization are negligible as compared to those of the Si $3p$ and Yb $5d$ valence states,[18] and the same is true for the conduction-band-state cross sections in IPES, which are related to the former by time reversal.[22] Figure 3 shows combined angle-integrated UPS and IPES results for $h\nu\simeq 10$ eV of the Yb-Si(111) interface and of Yb silicide, joined together at the Fermi level. This figure displays, therefore, a representation of the filled and empty DOS in the valence and conduction bands. Note that for the ordered (2×2) silicide, the curves shown are averages of angle-resolved spectra; nevertheless, the sharp maxima in the UPS spectrum originate from very strong **k**-conserving direct transitions that survive the averaging procedure.

The room-temperature Yb-Si interface (bottom curves of Fig. 3) reveals a high DOS at E_F and is considered, therefore, to be metallic. The maxima A_1 and B_1 in UPS and A_2 and B_2 in IPES are typical DOS features of RE metal-rich silicide-type interfacial compounds,[9,11–13,16,23,24] which have been interpreted in terms of bonding and antibonding metal-Si combinations. Upon heating to 250 °C, the DOS at E_F decreases and the intensity maxima move away from E_F. This trend is reinforced in the (2×2) silicide (top curves in Fig. 3) if the direct transition features in UPS are disregarded. The DOS at E_F in the epitaxial disilicide is very low and this compound appears to be semimetallic rather than metal-

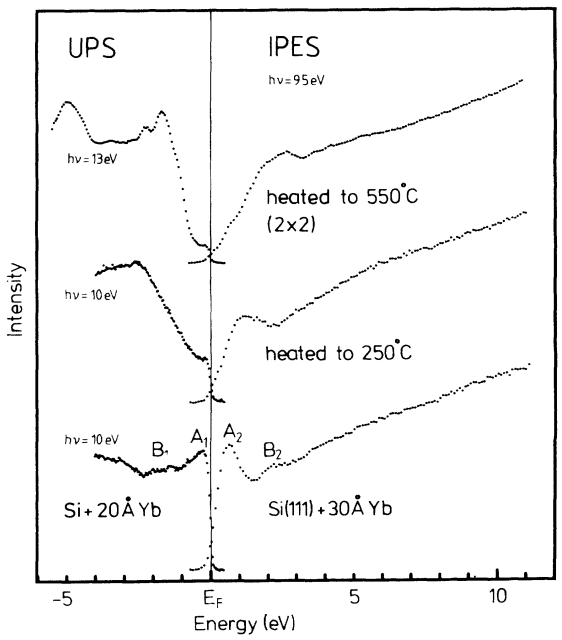

FIG. 3. Angle-averaged UPS and IPES spectra of Yb on Si(111) and of the heated interfaces. Note the low $h\nu$ in UPS, which matches the IPES isochromat energy.

lic. A similar behavior has been encountered at the Eu-Si(111) interface[13] which, in turn, showed close parallels to the Ca silicides.[25,26] The UPS and IPES curves of Fig. 3 also exhibit remarkably similar trends to those reported for the sequence of Ca silicides from Ca_2Si to $CaSi_2$:[25,26] as seen here, the structures corresponding to A move away from E_F with increasing silicon content of the silicide.

k-resolved IPES spectra of (2×2) Yb disilicide are presented in Fig. 4 as a function of the electron incidence angle θ. The silicide had been grown by evaporation of 50-Å Yb onto the heated Si(111) substrate, and showed a well-ordered LEED pattern. The angle θ is varied along the $[11\bar{2}]$ crystal azimuth, thus probing **k** in the $\bar{\Gamma}$-$\bar{M}$ direction of the Si(111) surface Brillouin zone, as indicated in the inset of Fig. 4. As a result of **k**-conserving direct transitions, a number of dispersing features can be observed when the θ angle is changed. Comparison of the results of Fig. 4 with those of an equivalent plot from an epitaxial (2×2) Eu silicide reported previously[13] reveals interesting coincidences in the behavior of dispersing features and, thus, a close relationship between the two systems. The peaks are sharper and better defined in the epitaxial Yb silicide than in the corresponding Eu silicide, and a number of additional features are evident in Fig. 4; this is the result of the improved ordering achieved by the present preparation procedure.

Normal-emission ($\theta=0°$) UPS spectra of the (2×2) Yb disilicide recorded as a function of photon energy between 10 and 23 eV are displayed in Fig. 5. The spectra are complex with many dispersing features, and we have attempted to guide the eye with dashed lines; however, other correlations are also possible. The Yb 4f emission is not clearly apparent in Fig. 5 for $h\nu<20$ eV, but it is expected at the indicated positions for $h\nu>20$ eV. In view of the previously mentioned similarities between Yb-Si and Ca-Si systems, it is tempting to investigate Ca-Si electronic structure calculations in the present context. Assuming epitaxial relationship with a hexagonal basal plane parallel to the Si(111) surface, normal-emission UPS would probe a line in the three-dimensional Brillouin zone along a Γ-A direction of a hexagonal unit cell.[27] Inspecting the band-structure calculations of Fahy and Hamann for $CaSi_2$ (Ref. 28) in their Γ-A direction shows two bands in the energy region of present interest, i.e., up to 4 eV, one of which is strongly dispersing and crosses E_F near A, whereas the other one is almost constant in energy near 2 eV. We observe a prominent, weakly dispersing feature just above 2 eV in Fig. 5, but otherwise very complex behavior between 1 and 2 eV. The situation near E_F is difficult to gauge because of possible interference with Yb 4f states, but the weakly dispersing feature at 0.2–0.3 eV below E_F for low $h\nu$ is

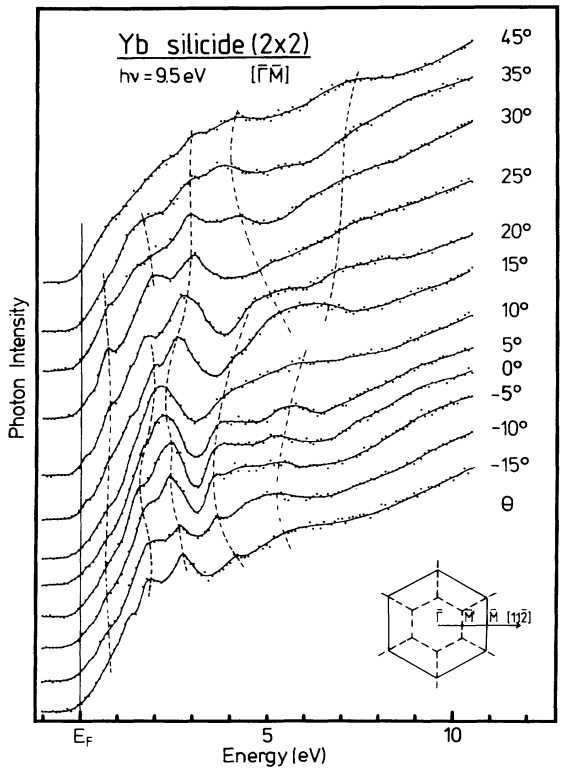

FIG. 4. **k**-resolved IPES spectra as a function of the electron incidence angle of the epitaxially grown (2×2) Yb disilicide. The inset gives the (1×1) and (2×2) surface Bruillouin zones and the probing direction. The dashed lines are guides to the eye to illustrate dispersing features.

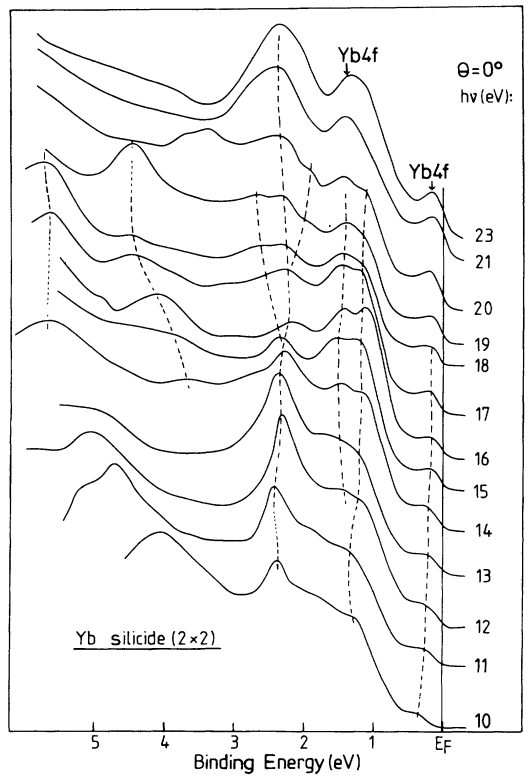

FIG. 5. **k**-resolved normal-emission UPS spectra of (2×2) Yb disilicide as a function of photon energy. The dashed lines are guides to the eye to indicate possible correlations of dispersing features. p-polarization.

not reflected in the $CaSi_2$ calculations. The analogies between Yb silicide and $CaSi_2$ should therefore not be overemphasized. Moreover, since the structure of the epitaxial (2×2) Yb silicide is not yet known, we refrain from further speculations in this direction until structure data and calculations, specifically for this system, are available. We do want to emphasize, however, that the k-resolved measurement presented in Figs. 4 and 5 are a convincing manifestation of the structural order in this epitaxial Yb silicide phase.

C. Electron-energy-loss spectroscopy

The electronic excitation spectra of the Yb-Si system as probed by EELS are presented in (a) $N(E)$ and (b) d^2N/dE^2 form in Fig. 6. These data complement the combined UPS-IPES results in Fig. 3, but also provide supplementary information. The top curves of Fig. 6 show as a reference EELS of Si(111) 7×7; these spectra, in particular the d^2N/dE^2 curve, are in excellent agreement with the pioneering EELS work of Ibach and Rowe,[29] in which all the transitions have been assigned consistently in terms of surface (*SS*) and bulk (*E*) interband and plasmon ($\hbar\omega_s$ and $\hbar\omega_p$) excitations. The loss spectrum of 30-Å Yb on Si(111), i.e., of the room-temperature interface, is dominated by the prominent Yb transitions at $\simeq 4$ and $\simeq 9$ eV.[30,31] The 4-eV loss peak has been interpreted previously[30] in terms of Yb $4f \rightarrow 5d$ one-electron excitations and the broad 9-eV feature as the combined surface and bulk plasmons of the divalent Yb surface. It is of interest to relate the $\simeq 4$-eV transition of the Yb-Si interface to the SXPS and UPS-IPES results obtained in the present work. The center of gravity of the $4f$ emission of the Yb-Si interface is at $\simeq 3$ eV below E_F as seen in Fig. 2, and excitation to the Yb $5d$-related DOS $\simeq 1$ eV above E_F (A_2 in Fig. 3) should yield an excitation peak energy of $\simeq 4$ eV; this is consistent with the experimental observation, in particular if the broad structure and the onset of loss intensity at $\simeq 2$ eV is considered, but it requires only weak electron-hole Coulomb interaction, which probably reflects the band character of the empty conduction-band states.

In the (2×2) Yb silicide the EELS spectra are notably different: the 4-eV structure is now very weak [barely seen in $N(E)$, but still recognizable in d^2N/dE^2], the Yb plasmon has given way to two features at 6.7 and 12.5 eV, and at $\simeq 17.5$ eV, a pronounced structure is observed. Interpretation of this behavior may be assisted by Fig. 3. The empty DOS is shifted away from E_F and the Yb $5d$ character is "diluted" by hybridization with Si $3p$ to form antibonding Yb-Si states in going from the room-temperature interface to the disilicide. This modification of the final states results in reduced oscillator strength for the $4f \rightarrow 5d$ transition. The 6.7-eV loss may be ascribed to an interband transition within the framework of Fig. 3, whereas the 12.5-eV feature is most likely to be associated with a silicide plasmon as observed on other RE silicides.[32,33] Strictly speaking, it should correspond to the surface solution within a simple layer model of the silicide on top of a Si substrate,[33,34] with the corresponding silicide-Si interface plasmon solution at higher energy at around 17 eV. However, in view of the evolution of the

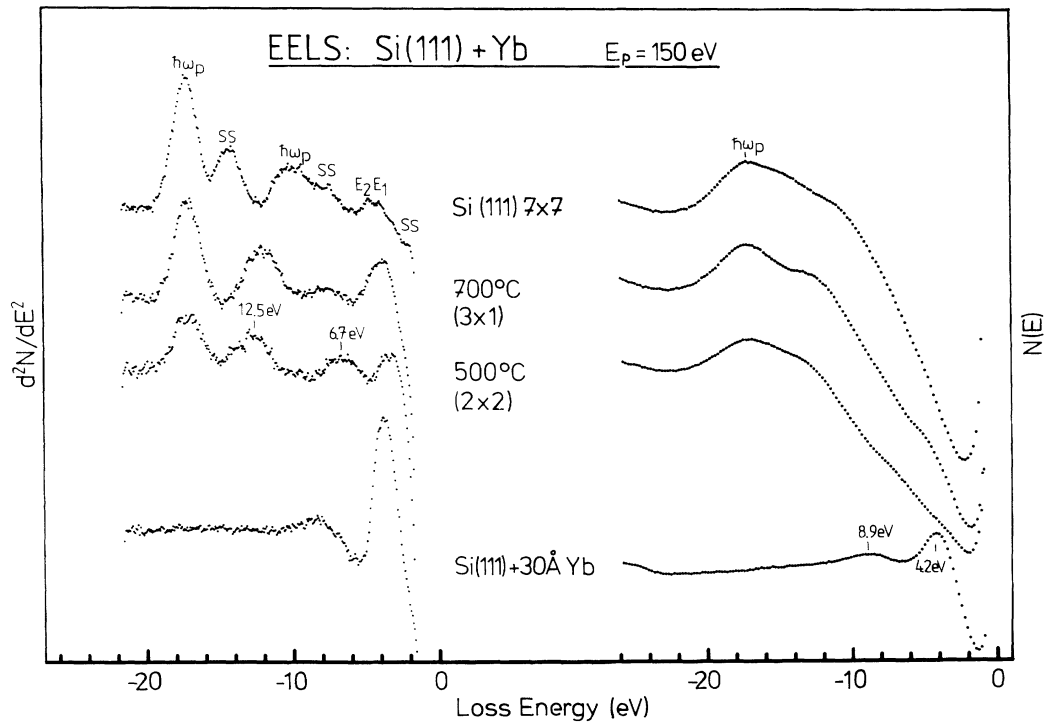

FIG. 6. Electron-energy-loss spectra of Si(111) 7×7 and of various Yb-Si systems as indicated in (a) $N(E)$ and (b) d^2N/dE^2 forms. The spectra have been recorded in approximate specular-reflection geometry.

loss spectra in Fig. 6, in particular in going from the (2×2) silicide via the (3×1) superstructure to the clean Si surface, we believe that the 17.5-eV loss structure seen on the heated samples is more likely related to the bulk plasmon of Si. The EELS spectra may then contain interesting information on the morphology of the expitaxial silicide phase. The inelastic mean free path of $\simeq$130-eV electrons is of the order of 10 Å,[35] and thus the Si plasmon should not be detectable through a >30-Å-thick silicide layer with the intensity observed in Fig. 6 unless the layer is not uniform. The EELS results therefore suggest that the epitaxial Yb disilicide phase is not grown in a uniform layer but rather in form of an island-related structure. LEED cannot be used to reveal surface topography on larger scales if the ordered islands are >100 Å^2 (the coherence area of the electron beam), but confirmation of the topography of epitaxial RE silicide phases will have to await investigations by more direct means such as, e.g., scanning tunneling microscopy.

IV. SUMMARY

Epitaxially well-ordered Yb silicides have been grown on Si(111) by solid-state epitaxy of room-temperature deposited Yb films on Si(111)7×7 via annealing to $\simeq500$ °C or by direct Yb evaporation onto Si(111) substrates heated to 250 °C–350 °C . The latter preparation method gave better ordering as judged by the dispersion in **k**-resolved electron spectroscopies. The SXPS spectra of $4f$ emission of the epitaxial Yb silicide give evidence of a valence-fluctuating configuration of Yb atoms in that phase, and, by comparison with literature data of Yb bulk silicides,[14] suggest a disilicide stoichiometry. The absence of surface components in the $4f$ emission of the epitaxial silicide phase is interpreted in terms of a structure model that involves pure Si with vacancies as the terminating surface layer; the ordering of vacancies gives rise to a (2×2) or sometimes a $(\sqrt{3}\times\sqrt{3})R30°$ LEED pattern.

The electronic structure of epitaxial Yb disilicide has been investigated by combining uv photoemission and inverse photoemission and by electron-energy-loss spectroscopy. The DOS diagrams of filled and empty states reveal a high DOS at E_F for the reacted Yb-Si room-temperature interface and, thus, metallic behavior, but a low DOS at E_F for the epitaxial silicide and more semimetallic character. The electronic excitation spectra are readily understood with the help of the DOS diagrams for one-electron transitions and in terms of plasmon excitations, but in addition the EELS spectra reveal information on the topography of the layer and suggest an island structure of the Yb disilicide phase.

k-resolved uv photoemission and inverse photoemission spectra of the (2×2) silicide phase have been recorded as a function of incidence electron angle and of photon energy. Many complex dispersing features are observed which, therefore, clearly demonstrate the epitaxial order in this phase, but detailed interpretation is hampered at the present time because of the lack of structure data and band-structure calculations.

ACKNOWLEDGMENTS

This experimental program has been supported by the Fonds zur Förderung der wissenschaftlichen Forschung of Austria. We are grateful to the BESSY staff for support during the measurements involving synchrotron radiation.

*Present address: Institut für Experimentalphysik, Karl-Franzens-Universität Graz, Universitätsplatz 5, A-8010 Graz, Austria.

[1]R. D. Thompson and K. N. Tu, Thin Solid Films **93**, 265 (1982).
[2]G. Rossi, Surf. Sci. Rep. **7**, 1 (1987).
[3]J. A. Knapp and S. T. Picraux, Appl. Phys. Lett. **48**, 466 (1986).
[4]W. A. Henle, M. G. Ramsey, F. P. Netzer, R. Cimino, and W. Braun, Solid State Commun. **71**, 657 (1989).
[5]F. Arnaud D'Avitaya, A. Perio, J.-C. Oberlin, Y. Campidelli, and J. A. Chroboczek, Appl. Phys. Lett. **54**, 2198 (1989).
[6]J.-Y. Duboz, P.-A. Badoz, A. Perio. J.-C. Oberlin, F. Arnaud D'Avitaya, Y. Campidelli, and J. A. Chroboczek, Appl. Surf. Sci. **38**, 171 (1989).
[7]M. P. Siegal, F. H. Kaatz, W. R. Graham, J. J. Santiago, and J. Van der Spiegel, Appl. Surf. Sci. **38**, 162 (1989).
[8]R. Baptist, S. Ferrer, G. Grenet, and H. C. Poon, Phys. Rev. Lett. **64**, 311 (1990).
[9]W. A. Henle, M. G. Ramsey, F. P. Netzer, and K. Horn, Surf. Sci. **254**, 182 (1991).
[10]C. Wigren, J. N. Andersen, R. Nyholm, and U. O. Karlsson, J. Vac. Sci. Technol. **A9**, 1942 (1991).
[11]P. Wetzel, L. Haderbache, C. Pirri, J. C. Peruchetti, D. Bolmont, and G. Gewinner, Surf. Sci. **251/252**, 799 (1991).
[12]W. A. Henle, M. G. Ramsey, F. P. Netzer, S. Witzel, and W. Braun, Surf. Sci. **243**, 141 (1991).
[13]R. Hofmann and F. P. Netzer, Phys. Rev. B **43**, 9720 (1991).
[14]I. Abbati, L. Braicovich, U. del Pennino, C. Carbone, J. Nogami, J. J. Yeh, I. Lindau, A. Iandelli, G. L. Olcese, and A. Palenzona, Phys. Rev. B **34**, 4250 (1986); Solid State Commun. **62**, 35 (1987).
[15]L. Braicovich, I. Abbati, C. Carbone, J. Nogami, and I. Lindau, Surf. Sci. **168**, 193 (1986).
[16]W. A. Henle, F. P. Netzer, R. Cimino, and W. Braun, Surf. Sci. **221**, 131 (1989).
[17]I. Chorkendorff, J. Kofoed, and J. Onsgaard, Surf. Sci. **152/153**, 749 (1985).
[18]J. J. Yeh and I. Lindau, At. Nucl. Data Tables **32**, 1 (1985).
[19]W. C. Lang, B. D. Padalia, D. J. Fabian, and L. M. Watson, J. Electron Spectrosc. Relat. Phenom. **5**, 207 (1974).
[20]S. F. Alvarado, M. Campagna, and W. Gudat, J. Electron Spectrosc. Relat. Phenom. **18**, 13 (1980).
[21]K. H. L. Buschow, M. Campagna, and G. K. Wertheim, Solid State Commun. **24**, 253 (1977).
[22]Th. Fauster and F. J. Himpsel, Phys. Rev. B **30**, 1874 (1984).

[23]E. Puppin, J. Nogami, C. Carbone, Z. X. Shen, I. Lindau, B. B. Plate, I. Abbati, and L. Braicovich, J. Vac. Sci. Technol. B **5**, 1083 (1987).
[24]C. Chemelli, S. Luridiana, M. Sancrotti, L. Braicovich, F. Ciccacci, A. Iandelli, G. C. Olcese, and A. Palenzona, Phys. Rev. B **42**, 1829 (1990).
[25]O. Bisi, L. Braicovich, C. Carbone, I. Lindau, A. Iandelli, G. L. Olcese, and A. Palenzona, Phys. Rev. B **40**, 10 194 (1989).
[26]C. Chemelli, M. Sancrotti, L. Braicovich, F. Ciccacci, O. Bisi, A. Iandelli, G. L. Olcese, and A. Palenzona, Phys. Rev. B **40**, 10 210 (1989).
[27]The assumption here is a $CaSi_2$-type structure as depicted by Fahy and Hamann in Ref. 28.
[28]S. Fahy and D. R. Hamann, Phys. Rev. **41**, 7587 (1990).
[29]H. Ibach and J. E. Rowe, Phys. Rev. B **10**, 710 (1974).
[30]E. Bertel, G. Strasser, F. P. Netzer, and J. A. D. Matthew, Surf. Sci. **118**, 387 (1982).
[31]F. P. Netzer, G. Strasser, G. Rosina, and J. A. D. Matthew, Surf. Sci. **152/153**, 757 (1985).
[32]W. A. Henle, M. G. Ramsey, and F. P. Netzer, Vacuum **41**, 814 (1990).
[33]W. A. Henle, Ph.D. thesis, University of Innsbruck, 1990.
[34]L. J. Brillson, Phys. Rev. Lett. **38**, 245 (1977).
[35]M. P. Seah and W. A. Dench, Surf. Interf. Anal. **1**, 2 (1979).

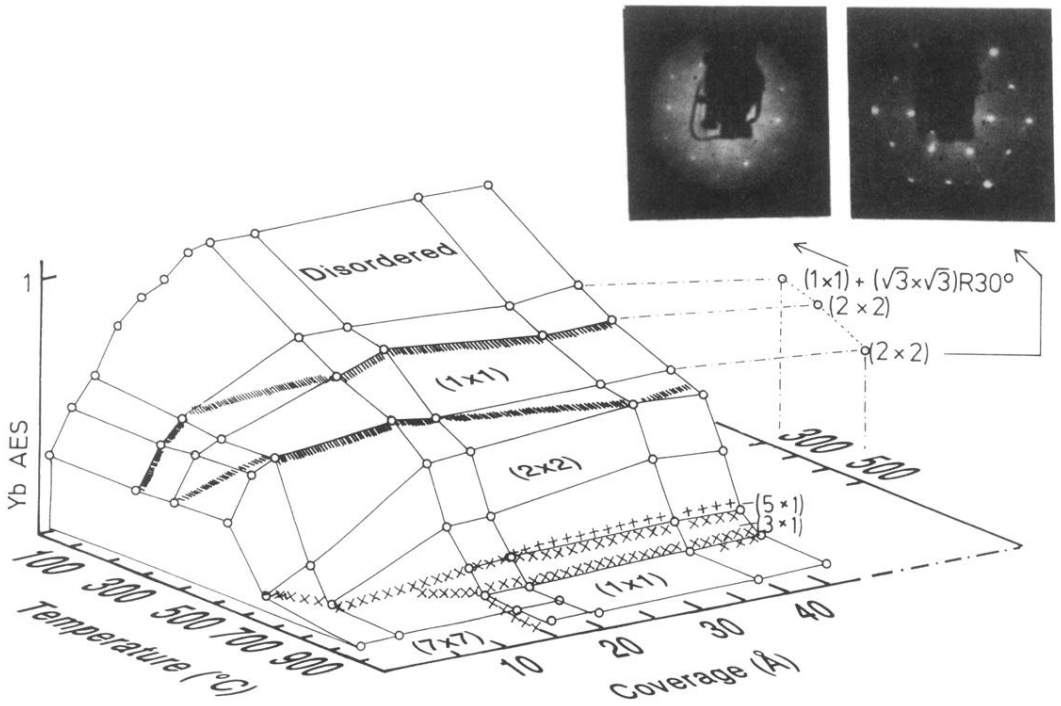

FIG. 1. Phase diagram of the Yb-Si(111) interface in the form of a plot of the Yb Auger signal vs temperature as a function of Yb coverage (1 monolayer is equal to 3.2 Å). Experimental points are symbolized by the open circles, and regions of ordered LEED structures are indicated. The data points to the right of the main three-dimensional diagram have been obtained by evaporation of 50 Å Yb onto heated Si substrates. The LEED photographs have been taken from these latter phases.